Nuclear Engineering and Technology 48 (2016) 200–210

Available online at ScienceDirect

Nuclear Engineering and Technology

journal homepage: www.elsevier.com/locate/net

Original Article

Characterization of a Neutron Beam Following Reconfiguration of the Neutron Radiography Reactor (NRAD) Core and Addition of New Fuel Elements

Aaron E. Craft [a,*], *Bruce A. Hilton* [b], *and Glen C. Papaioannou* [a]

[a] *Idaho National Laboratory, 2525 Fremont Ave., Idaho Falls, ID 83415, USA*
[b] *TerraPower, LLC, 330 120th Avenue NE, Suite 100, Bellevue, WA 98005, USA*

ARTICLE INFO

Article history:
Received 19 May 2015
Received in revised form
19 October 2015
Accepted 20 October 2015
Available online 2 December 2015

Keywords:
Beam Characterization
Neutron Radiography
Neutron Beam

ABSTRACT

The neutron radiography reactor (NRAD) is a 250 kW Mark-II Training, Research, Isotopes, General Atomics (TRIGA) reactor at Idaho National Laboratory, Idaho Falls, ID, USA. The East Radiography Station (ERS) is one of two neutron beams at the NRAD used for neutron radiography, which sits beneath a large hot cell and is primarily used for neutron radiography of highly radioactive objects. Additional fuel elements were added to the NRAD core in 2013 to increase the excess reactivity of the reactor, and may have changed some characteristics of the neutron beamline. This report discusses characterization of the neutron beamline following the addition of fuel to the NRAD. This work includes determination of the facility category according to the American Society for Testing and Materials (ASTM) standards, and also uses an array of gold foils to determine the neutron beam flux and evaluate the neutron beam profile. The NRAD ERS neutron beam is a Category I neutron radiography facility, the highest possible quality level according to the ASTM. Gold foil activation experiments show that the average neutron flux with length-to-diameter ratio (L/D) = 125 is 5.96×10^6 n/cm^2/s with a 2σ standard error of 2.90×10^5 n/cm^2/s. The neutron beam profile can be considered flat for qualitative neutron radiographic evaluation purposes. However, the neutron beam profile should be taken into account for quantitative evaluation.

1. Introduction

The neutron radiography reactor (NRAD) is a 250 kW Mark II Training, Research, Isotopes, General Atomics (TRIGA) research reactor located beneath the main hot cell of the Hot Fuel Examination Facility (HFEF) at Idaho National Laboratory, Idaho Falls, ID, USA. The NRAD is equipped with two neutron beamlines, which route from the NRAD into separate shielded

* *Corresponding author.*
E-mail address: aaron.craft@inl.gov (A.E. Craft).

http://dx.doi.org/10.1016/j.net.2015.10.006
1738-5733/Copyright © 2015, Published by Elsevier Korea LLC on behalf of Korean Nuclear Society.

radiography stations in the lower level of the HFEF, the East Radiography Station (ERS) and the North Radiography Station (NRS) [1]. The ERS and NRS neutron beamlines are designed and primarily used for neutron radiography of nuclear fuels. The ERS sits directly beneath the HFEF hot cell, and an elevator within the hot cell remotely positions a fuel specimen into the ERS for neutron radiography. The NRS is not directly beneath the HFEF hot cell, and a cask system is used to transport fuel to the NRS high bay, and an elevator remotely positions the fuel into the NRS for neutron radiography. Fuel development programs are the primary users of the ERS for neutron radiography, and characterization of the ERS neutron beam provides valuable information describing the quality of the neutron beam for performing neutron radiography.

Previous studies examined various characteristics of the ERS neutron beam, including the beam length-to-diameter (*L/D*) ratio, beam divergence, and a calculated representative energy spectrum [2,3]. The previous studies also followed American Society for Testing and Materials (ASTM) standards to determine the category of the radiography facility, which provides a means to compare the quality of different neutron radiography facilities [4]. Unfortunately, the *L/D* ratio was unable to be determined in the previous study, but it should be close to 125, which is the *L/D* based on the diameter of the aperture and the distance between the aperture and image plane. The neutron flux at the image plane was determined to be $5.54 \times 10^6 \pm 5.5 \times 10^5$ n/cm^2/s [2]. Additionally, the previous study determined that the ERS neutron radiography facility was a category I facility, which is the highest possible quality level in the ASTM standard [2].

The Reduced Enrichment for Research and Test Reactors Program, in support of the Global Threat Reduction Initiative, required conversion of all civilian reactor facilities from highly enriched uranium ($\geq$ 20% ^{235}U) to low enriched uranium fuel (< 20% ^{235}U). The NRAD was converted to low enriched uranium fuel beginning in August 2009 and was completed in June 2010 [5]. Because the core excess reactivity was less than predicted and would not allow for extended operations, an additional four fuel elements and four graphite elements were added to the NRAD reactor core in 2013 to increase the excess reactivity of the reactor, which may have changed some characteristics of the neutron beamline [5]. The addition of fuel elements to the core does not affect the geometry of the neutron beam (e.g., aperture, collimator, ERS/NRS cells) and thus should not affect the *L/D* ratio or divergence. However, additional fuel in the reactor core could affect the neutron flux magnitude and energy spectrum, and therefore may affect the quality of the neutron radiographs produced by the facility. The work described in this manuscript seeks to assess the impact, if any, of the reactor modification on the radiographic quality of the facility by determining the ASTM category of the neutron imaging system. Additionally, this work includes determination of the neutron beam profile using an array of gold foils and a film image of the unimpeded neutron beam.

The next section describes the neutron imaging capabilities currently used at the NRAD, followed by a discussion of the work to determine the facility category according to ASTM standards, and finally a discussion of the neutron beam flux determination and beam profile mapping.

2. Neutron radiography at the NRAD

Radiography is a nondestructive testing method which produces a radiographic image using penetrating radiation, such as X-rays or neutrons, instead of visible light. The attenuation of a radiation beam passing through an object reveals clues about the internal structure of that object. X-ray and gamma radiation are attenuated through interactions with electrons; accordingly, the radiation attenuation coefficient increases continuously with increasing atomic number [6]. Neutrons, however, interact with nuclei rather than orbital electrons, and the probability of interaction is determined by both the incident neutron energy and the detailed structure of the target nucleus, which differs for each isotope [7]. Fig. 1 depicts a qualitative representation of both X-ray and neutron attenuation cross-sections for some common elements. In each case, the area of the circle is proportional to the corresponding attenuation cross-section.

X-ray and neutron radiography are complementary, and one technique should not be universally utilized or excluded over the other. The most appropriate technique for evaluating a specimen depends on the geometry and material chemical and isotopic composition of the particular specimen. The radioactivity is characteristic of the isotopic composition of the specimen. For nuclear fuel, X-ray radiography is extremely challenging, primarily because the large amount of gamma radiation coming from the fuel degrades X-ray radiographic images. By comparison, some neutron radiography techniques are not sensitive to the gamma radiation from nuclear fuel, and are capable of producing high quality images of nuclear fuel. Neutron radiography can provide valuable information regarding the condition of nuclear fuel, such as fuel swelling, pellet-clad interactions, pellet cracking, fuel central-void formation, evidence of fuel melting, and migration of material [8–14]. No other nondestructive testing technique provides a comparable amount of comprehensive information on the condition of nuclear fuel than neutron radiography [8].

There are a number of methods for producing images with neutrons including: (1) direct and indirect radiography using activation foils and X-ray film [15]; (2) digital radiography using image storage plates and a scanner [16]; (3) real-time scintillating screens with a Charge-coupled device (CCD) camera [17]; (4) neutron-sensitive multichannel plates [18,19]; (5) the track-etch method [15], and others. For the NRAD, the high gamma dose rates coming from used fuel specimens (typically between 10^3 R/h and 10^6 R/h) prohibits most neutron

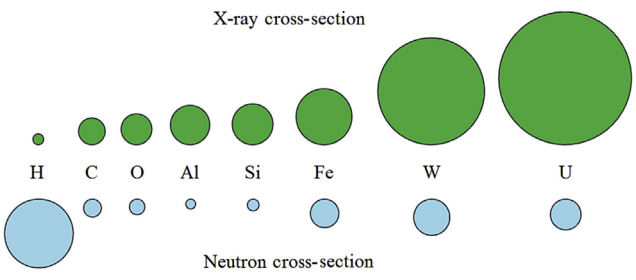

Fig. 1 – X-ray and neutron cross-sections of some common elements.

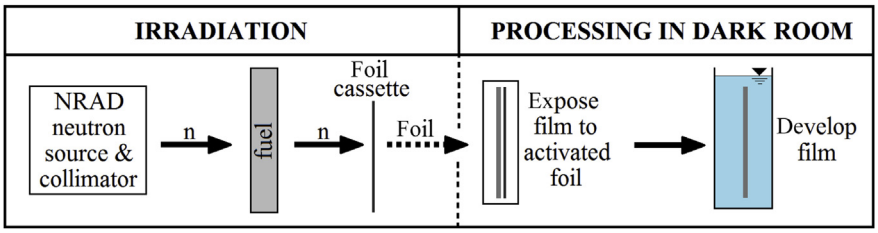

Fig. 2 – Schematic of the indirect neutron radiography process.

radiography techniques. Many of these radiographic techniques are sensitive to ionizing radiation, including high energy photons (e.g., X-rays and gamma radiation), and thus are not appropriate for imaging used fuel. However, indirect (or transfer method) neutron radiography is not gamma-sensitive, and is the only radiographic technique widely used for imaging irradiated nuclear fuel.

Indirect (or transfer) method neutron radiography involves the use of an intermediate detector, which produces an image upon subsequent processing. For this technique, a metal foil (e.g., dysprosium, indium) is used as the image recorder; the foil captures the image as activation of the foil material [15]. Fig. 2 shows a schematic of the indirect radiography process [20]. An activation foil is placed behind an object of interest (e.g., used nuclear fuel) and absorbs neutrons that penetrate through the object and subsequently becomes activated. After irradiation, the activated foil is taken to a dark room where it is placed in contact with an X-ray film. The decay radiation exposes the film according to the pattern of activation of the foil. Subsequent development of the film produces a neutron radiograph of the object.

The NRAD routinely performs neutron radiography using the transfer method with dysprosium and indium activation foils and X-ray film. The NRAD has also performed transfer method neutron radiography with dysprosium and indium activation foils and scintillation screens and reader [21]. A cassette is loaded with a dysprosium foil, then a cadmium foil, followed by an indium foil and another cadmium foil, in this order (Fig. 3). The cassette is loaded onto a transporter

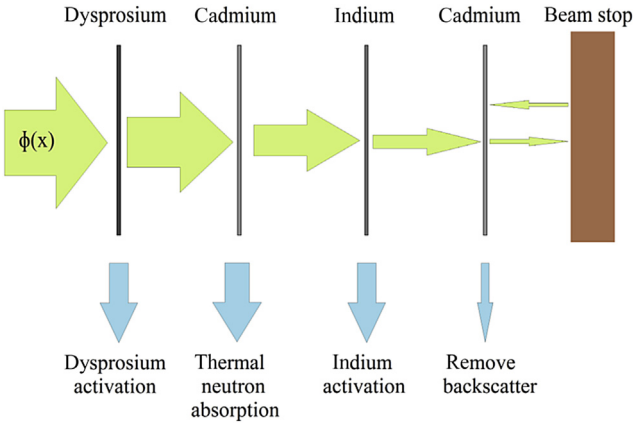

Fig. 3 – Schematic depicting the absorption of a neutron beam by activation foils within a cassette.

that remotely positions the cassette behind the ERS specimen elevator. The neutron beam passes through a specimen loaded in the ERS elevator (e.g., a fuel element) and activates the foils in the cassette according to the pattern of attenuation of the neutron beam. The dysprosium foil becomes activated primarily by thermal neutrons. A cadmium foil is placed between the dysprosium and indium foils to filter out low energy neutrons (approximately < 0.5 eV), effectively exposing the indium foil to only epithermal neutrons (Fig. 3). A final cadmium foil removes any backscattered neutrons that could produce noise in the radiographs. Thus, in one exposure, the NRAD produces two radiographs from thermal and epithermal neutrons. The differences in material cross-sections at thermal and epithermal energies allow users to visualize different features of interest from each of the radiographs.

After exposure, the activated dysprosium and indium foils are taken into a dark room, and X-ray film is placed in contact with the foils in a vacuum-sealed, light tight cassette. The dysprosium and indium foils decay and release beta radiation, which exposes the adjacent film in the same pattern of the foil activation. Subsequent development of the film produces a film image of the specimen, which is scanned with a high resolution scanner to produce a digital image.

3. Neutron beam quality

The potential quality of an image produced with a neutron beam can be determined by comparing an image of a test object with an image of a similar object that contains known artificial discontinuities [22]. In common practice, an image quality indicator (IQI) developed by the ASTM, often called a sensitivity indicator (SI), emulates defects of varying size, with gaps between and holes placed beneath different thicknesses of acrylic resin [4]. The SI is a reasonable IQI to simulate general defects, but a more representative specimen is typically more desirable for specific applications. For example, a calibration fuel pin is a more representative IQI for neutron radiography of nuclear fuel than the SI [20]. A second IQI is a beam purity indicator (BPI), which produces information concerning the neutron beam and imaging system parameters that contribute to overall image quality. Following the ASTM standard procedure determines a facility category classification that allows users to compare radiography facilities.

4. ASTM IQIs

ASTM standards provide guidelines for the construction of the SI [23] and the BPI [24]. The SI is an aluminum u-channel filled with alternating strips of methyl methacrylate and aluminum, which are milled into steps (Fig. 4). The aluminum strips (T-Z) simulate gaps and range from 0.254 mm to 0.0127 mm thick. There are four methyl methacrylate shims beneath the thicker methyl methacrylate steps, and holes in these shims (1–12) simulate defects and range from 0.508 mm to 0.0127 cm in diameter. A radiograph of the SI is taken and the quantitative determination of the radiographic quality is determined by visually inspecting the SI for the number of visible simulated defects (e.g., holes and gaps) [4].

The BPI is constructed of a block of polytetrafluoroethylene with a hole cut out of its center, and contains two boron nitride discs, two lead discs, and two cadmium wires (Fig. 5). A combination of each material is mounted on the top and bottom faces of the block. Optical density measurements listed in Table 1 are taken from the radiograph of the BPI in locations indicated by the variables shown in Fig. 5A. These values are applied to equations from the ASTM standard to determine beam quality metrics that determine the facility category [4].

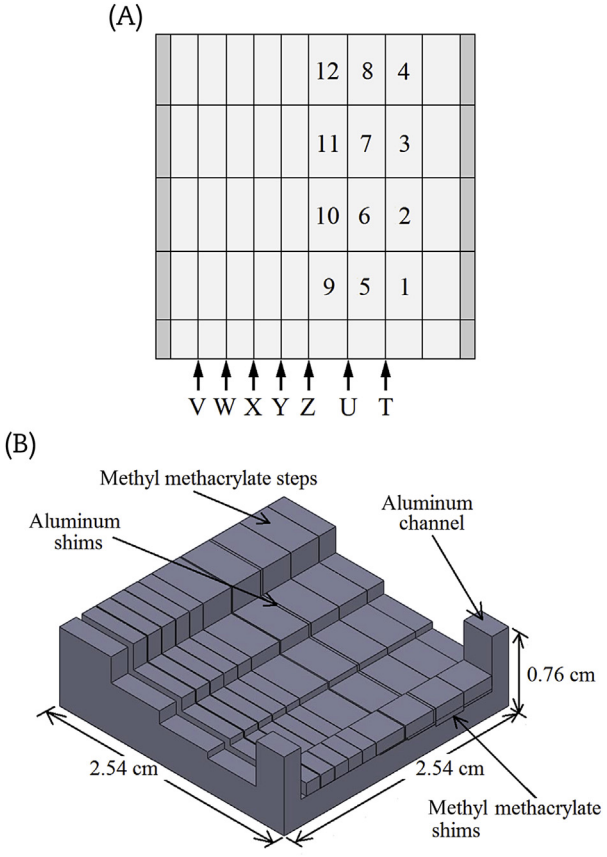

Fig. 4 – Schematic of the sensitivity indicator. (A) Top-view of the sensitivity indicator; (B) perspective view of the sensitivity indicator.

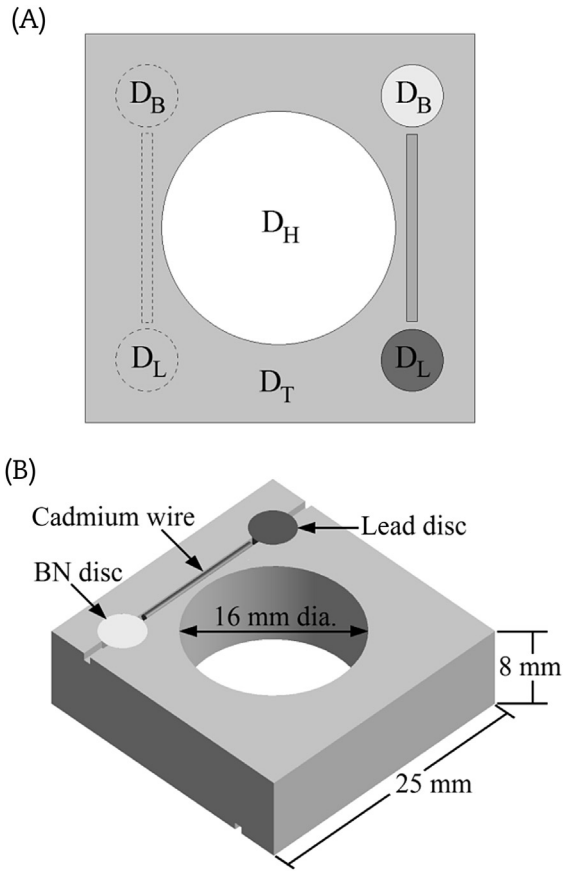

Fig. 5 – Schematic of the beam purity indicator. (A) Top-view of the beam purity indicator; (B) perspective view of the beam purity indicator.

5. Evaluation of the ERS radiographic facility quality level

Measurements taken from visual inspection of a radiograph of the SI and optical density measurements taken from the radiograph of the BPI provide parameters necessary for determining the category of the radiography facility. Table 2 lists the beam parameters that determine the facility category, where a category I facility is the top rating [4]. The parameters in the table represent different measures of beam quality, where *NC* is the thermal neutron content, *H* is the smallest hole visible in the SI, *G* is the smallest gap visible in the SI, *S* is the scattered neutron content, γ is the gamma content, and *P* is the pair production content.

Eqs. (1) and (2) determine the effective thermal neutron content (*NC*) and effective scattered neutron content (*S*). In addition to the thermal and scattered neutron contents, the ASTM standard also gives equations for calculating gamma content and pair production, but these are only applicable when using direct method neutron radiography using gadolinium conversion foils. The NRAD performs indirect method radiography, so the gamma content and pair production parameters are not applicable. However, the remaining values are sufficient to determine the facility category [4]:

Table 1 – Definitions of film density parameters.

Parameter	Description
D_B	Film densities measured through the images of the boron nitride discs
D_L	Film densities measured through the images of the lead discs
D_H	Film density measured at the center of the hole in the BPI
D_T	Film density measured through the image of the polytetrafluoroethylene
ΔD_L	Difference between the D_L values
ΔD_B	Difference between the 2 D_B values

BPI, beam purity indicator.

$$NC = \frac{D_H - (higher\ D_B + \Delta D_L)}{D_H} \times 100 \quad (1)$$

$$S = \frac{\Delta D_B}{D_H} \times 100 \quad (2)$$

Table 3 lists the optical density values taken from a neutron radiograph of the BPI to determine the parameters listed in Table 1, including the effective thermal neutron content (NC) and the effective scattered neutron content (S). Relative error for each of the measurements is ± 3%. The film should have sufficient exposure such that the background optical density (D_H) is between 2.0 and 3.0 [4], and the background value for this examination is within this range at 2.47. The film density measurements are applied to Eqs. (1) and (2) to calculate NC and S, which are also listed in Table 3.

Upon visual inspection of the radiograph of the SI, seven holes are visible and the smallest gap in the SI (shim Z) is visible. Thus, the resulting value of H is 7, and the value of G is 7. These are combined with NC and S and listed in Table 4. Based on the ASTM standard, the NRAD ERS neutron radiography facility is a Category I facility.

Table 2 – Neutron radiographic categories and beam quality parameters [4].

Category	NC	H	G	S	γ	P
I	65	6	6	5	3	3
II	60	6	6	6	4	4
III	55	5	5	7	5	5
IV	50	4	5	8	6	6
V	45	3	5	9	7	7

γ, gamma content; G, the smallest gap visible in the sensitivity indicator (SI); H, the smallest hole visible in the SI; NC, the thermal neutron content; P, the pair production content; S, the scattered neutron content.

Table 3 – Beam quality parameter values.

Parameter[a]	Value
D_B	0.50 & 0.52
D_L	2.03 & 2.10
D_H	2.47
D_T	2.04
ΔD_L	0.07
ΔD_B	0.02
NC	78.1
S	0.8

NC, the thermal neutron content; S, the scattered neutron content.

[a] See Table 1 for definitions of film density parameters.

6. Neutron beam flux and beam profile

A neutron beam may not be uniform over the image plane due to source distribution, geometrical factors, and interactions between the beam and its surroundings. First, asymmetry in the neutron source penetrating the aperture will cause asymmetry in the beam profile. The neutron beam may interact with its surroundings in a way that affects the neutron beam profile. The neutron beam may scatter off the collimator walls or other items in the beam path which can cause variations in the beam profile, and backscatter off materials behind the image plane (often a beam stop) could affect the profile as well.

Another factor that affects the neutron beam profile is the effective collimation ratio (L/D), where L is the distance from the aperture to the image plane and D is the diameter of the aperture. A lower L/D results in a more serious blur on the image than that due to the inherent unsharpness of the imaging device [25]. As the L/D ratio increases, the unsharpness decreases and image quality improves. In addition to affecting the unsharpness of the image, the L/D ratio could affect the neutron beam profile. Due purely to geometrical parameters, the neutron beam profile appears increasingly flat at the image plane as L/D increases. The intensity peaks at the center of the beam at the image plane and decreases with distance from the center of the beam. These variations in the beam profile related to the L/D ratio are different than the unavoidable deterioration of image quality due to geometric blur that is also affected by the L/D ratio, but both of these effects become increasingly pronounced at lower L/D values [25].

Most of these effects can be mitigated through careful design of the neutron beam [25]. For applications where only qualitative analysis is required, a certain level of asymmetry in the neutron beam may be acceptable and require no image

Table 4 – Neutron radiographic category of the East Radiography Station (ERS) neutron radiography facility.

	NC	H	G	S
Category I Requirements	≥65	≥6	≥6	≤5
NRAD ERS Parameters	78.1	7	7	0.8

G, the smallest gap visible in the sensitivity indicator (SI); H, the smallest hole visible in the SI; NC, the thermal neutron content; NRAD, neutron radiography reactor; S, the scattered neutron content.

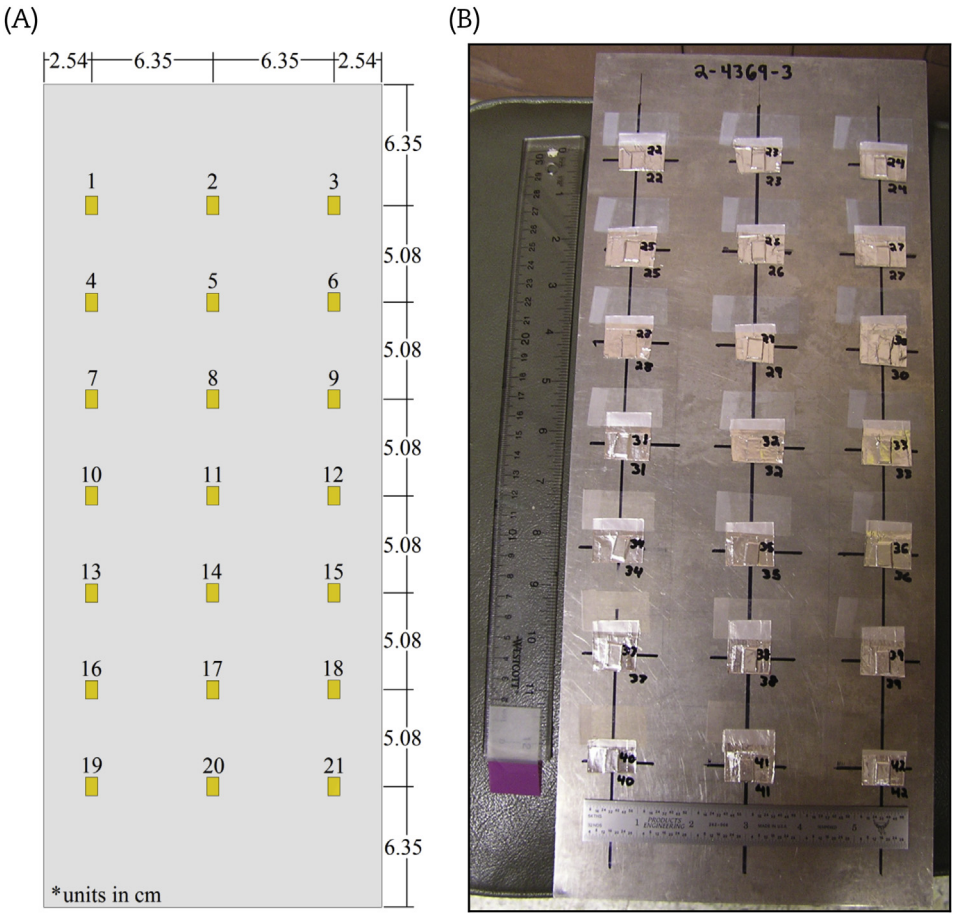

Fig. 6 – Array of gold foils for beam flux profile mapping. (A) Schematic of gold foil arrangement; (B) picture of gold foil arrangement.

processing to correct for the profile. However, it may be necessary to correct for the beam profile for some qualitative and most quantitative applications. This section describes the methods used to determine the neutron beam profile of the NRAD ERS neutron beam.

7. Fundamentals of measuring neutron flux

Radioactivation techniques obtain information by converting stable nuclei into radioactive nuclei and measuring the reaction products, and these techniques are used to determine the ERS neutron beam flux. In neutron activation analysis (NAA), a material bombarded with neutrons may release radiation nearly instantaneously and/or become radioactive [26]. The decay radiation from the activated specimen is then measured to determine desired information about the neutron field that activated the material. In this work, NAA using gold foils exposed to the NRAD ERS neutron beam determines the neutron beam intensity and beam profile.

Gold is a common material for measuring the neutron flux of a neutron beam using NAA. A gold foil is placed in a neutron beam and the neutrons activate the gold by a $^{197}Au(n,\gamma)^{198}Au$ absorption reaction with $\sigma_a = 98.69$ b and $\Sigma_a = 5.83$ cm^{-1} thermal absorption cross-sections [27,28]. The ^{198}Au is radioactive and decays with a ~2.695 day half-life [27,28]. After exposure to the neutron beam, the decay radiation is counted and the activity of the sample is calculated. The average neutron flux incident on the gold foil during exposure is then calculated by Eq. (3):

$$\overline{\phi} = \frac{M\,A(t)}{m\,N_A\,\gamma\,\sigma\,(1-e^{-\lambda t_{exp}})} \tag{3}$$

where M is the molar mass of the sample, $A(t)$ is the activity of the sample at the end of exposure, m is the mass of the foil, N_A is Avogadro's number, γ is the atom fraction of the isotope of interest, σ is the microscopic cross-section of the reaction of interest (absorption in this case), λ is the decay constant of the radioactive isotope of interest produced during exposure, and t_{exp} is the duration of exposure [29,30].

Neutrons are absorbed and scattered as they pass through the foil, and the neutron flux decreases exponentially with distance in the foil. This can become significant for thick foils and for materials with large attenuation cross-sections, and the incident neutron flux, ϕ_0, can be measurably larger than

Table 5 – Measured neutron flux values from neutron activation analysis of gold foils.

Foil Nos.	Distance from center (cm)		Neutron flux (n/cm^2/s)		Average neutron flux (n/cm^2/s)
	Horizontal	Vertical	Set 1	Set 2	
1 & 22	−6.35	15.24	5.63×10^6	5.64×10^6	5.64×10^6
2 & 23	0.00	15.24	5.76×10^6	6.37×10^6	6.07×10^6
3 & 24	6.35	15.24	5.67×10^6	6.05×10^6	5.86×10^6
4 & 25	−6.35	10.16	5.58×10^6	5.76×10^6	5.67×10^6
5 & 26	0.00	10.16	5.84×10^6	6.17×10^6	6.01×10^6
6 & 27	6.35	10.16	5.87×10^6	5.89×10^6	5.88×10^6
7 & 28	−6.35	5.08	5.84×10^6	5.96×10^6	5.90×10^6
8 & 29	0.00	5.08	5.93×10^6	5.99×10^6	5.96×10^6
9 & 30	6.35	5.08	5.80×10^6	5.96×10^6	5.88×10^6
10 & 31	−6.35	0.00	6.17×10^6	6.15×10^6	6.16×10^6
11 & 32	0.00	0.00	5.97×10^6	5.98×10^6	5.98×10^6
12 & 33	6.35	0.00	6.37×10^6	6.11×10^6	6.24×10^6
13 & 34	−6.35	−5.08	6.12×10^6	6.01×10^6	6.06×10^6
14 & 35	0.00	−5.08	6.23×10^6	6.02×10^6	6.13×10^6
15 & 36	6.35	−5.08	5.96×10^6	5.86×10^6	5.91×10^6
16 & 37	−6.35	−10.16	5.89×10^6	6.16×10^6	6.03×10^6
17 & 38	0.00	−10.16	5.88×10^6	5.99×10^6	5.93×10^6
18 & 39	6.35	−10.16	6.01×10^6	6.05×10^6	6.03×10^6
19 & 40	−6.35	−15.24	5.98×10^6	5.89×10^6	5.94×10^6
20 & 41	0.00	−15.24	6.06×10^6	6.12×10^6	6.09×10^6
21 & 42	6.35	−15.24	5.87×10^6	5.90×10^6	5.88×10^6
Average neutron flux			5.93×10^6	6.00×10^6	5.96×10^6
Relative error (2σ)			3.90×10^5	3.14×10^5	2.90×10^5

the average neutron flux calculated using Eq. (3) [26]. Neutron scattering for the materials and foil thickness used in this work are negligible. However, the absorption cross-section of gold (σ_a = 98.69 b) is large enough that it produces a substantial decrease in the neutron flux within the gold foil, and is accounted for using a correction factor, f, given in Eq. (4) [28]. If the effects of scattering were more pronounced, a modified correction factor would be required [31]:

$$f \equiv \frac{\overline{\phi}}{\phi_0}; \quad f = \frac{1 - e^{\Sigma x}}{\Sigma x} = \frac{1 - e^{-\frac{mN_A}{M}\sigma x}}{\frac{mN_A}{M}\sigma x} \tag{4}$$

Combining Eqs. (3) and (4), the incident neutron flux is calculated by Eq. (5):

$$\phi_0 = \frac{M\,A(t)}{f\,m\,N_A\,\gamma\,\sigma\,(1 - e^{-\lambda t_{exp}})} \tag{5}$$

8. Neutron flux profile using neutron activation techniques

One gold foil measurement using NAA produces one measurement of the neutron flux of a neutron beam. It is good practice to take multiple measurements to improve confidence in the measured value of the neutron flux. Furthermore, the neutron flux of the beam is not necessarily spatially constant, so an array of gold foils is used to produce a quantitative map of the neutron beam profile. In this study, two arrays of 21 gold foils are placed in the ERS neutron beam in a 3 × 7 array as shown in Fig. 6. Foils in the first set of 21 are labeled 1–21; the foils in the second set are labeled 22–42. The gold foils are each roughly 6.35 mm × 8.255 mm and 0.254 mm thick. For a pure gold foil 0.254 mm thick, the absorption correction factor is $f = 0.928$ using Eq. (4).

The array of gold foils is loaded into a cassette and remotely positioned behind the ERS elevator. The gold foils are exposed to the neutron beam for 1 hour. Following exposure, the foils are removed and transported to the Analytical Laboratory at the Materials and Fuels Complex, where the activated foils are counted to determine the activity of each foil after the exposure. The standard error (2σ) for the measured activities is ± 3%. Given the calculated activity at the end of exposure, $A(t)$, the measured mass of each gold foil, m, the calculated correction factor, f, and other known parameters of gold, the neutron flux incident on each gold foil is calculated using Eq. (5).

The exposure, counting, and flux calculation are performed for both sets of gold foils. The resulting neutron flux for each foil is listed in Table 5. Set 1 includes foils 1–21, and Set 2 includes foils 22–42. Foils 1 and 22 are in the same position in the array, and likewise for each set of corresponding foils. The average neutron flux in each position in the array is listed in the last column of Table 5. The average neutron flux is 5.96×10^6 n/cm^2/s, with a 2σ standard deviation of 1.79×10^5 n/cm^2/s.

Fig. 7 shows the deviation of the neutron flux from the average neutron flux for each foil position. Out of the 21 positions, the measured neutron flux at 17 positions fall within the 2σ relative error. The two lower flux measurements (Foils 1 and 4) are located in the upper left corner of the beam, indicating a lower neutron flux at that position. Foil positions 10 and 12 are near the center of the beam, and show a slightly higher neutron flux. This indicates a noticeable variation in the neutron beam profile, perhaps around 10% over the active beam area covered by the gold foil array.

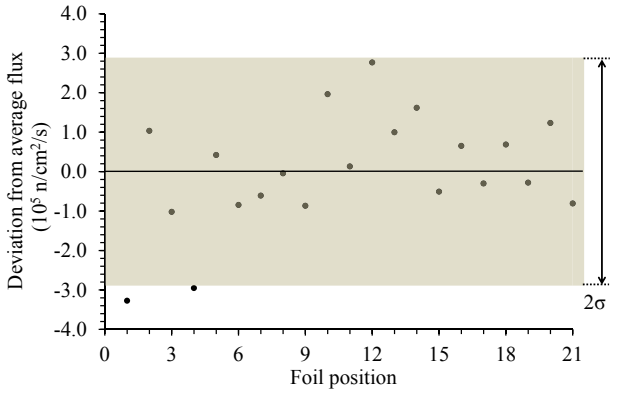

Fig. 7 – Deviation from the average neutron flux for each foil position.

9. Neutron beam profile from film radiographs

Gold foil activation experiments in the previous subsection revealed a noticeable variation in the neutron beam flux across the field of view. These measurements provide a flux magnitude, but the resulting profile is coarse, since there were only 21 data points over the image plane. Another way to produce a beam profile is to take a neutron radiograph of the neutron beam without a specimen loaded in the elevator. This section describes the acquisition and analysis of the beam profile taken from a neutron radiograph.

In neutron radiography, the neutron beam activates a dysprosium foil positioned behind the elevator. Once activated, the foil is placed in contact with film, and the decay radiation from the activated dysprosium exposes the film. The activation rate of the dysprosium foil is directly proportional to the impinging neutron flux and is also a function of the neutron energy spectrum. However, the activity of the dysprosium foil, and thus the neutron flux, is not directly proportional to the resulting film density of the exposed film. The relationship between the exposure of the film and the resulting film density is described by a film response curve, which is different for each type of film. Although not directly proportional, the grayscale values of the scanned film image correlate to the neutron flux; a low grayscale value (darker) indicates higher neutron flux.

To discern the effect of this profile on film radiographs, neutron radiographs are taken with no specimen loaded in the ERS elevator, producing a blank shot, commonly referred to as either a "background" or "light" image. The radiographs are scanned in a film scanner at 16-bit grayscale and 1,200 dpi. The light image from the scanned dysprosium radiograph is shown in Fig. 8. There is a noticeable decrease in film density (increased light transmittance) at the edges of the film, suggesting lower dysprosium activation and thus lower neutron flux at the edges of the field of view.

The variation in the background image in Fig. 8 is noticeable, but some details and magnitude of the variation of the neutron beam profile are not immediately apparent. To better distinguish the beam profile in the film, the scanned image is processed to produce a two-dimensional mesh plot and a

Fig. 8 – Background image from a dysprosium-exposed film.

contour plot, shown in Fig. 9. The mesh plot in Fig. 9A shows the peak-to-average ratio, and the contour plot in Fig. 9B is grayscale normalized to 1 in 16-bit grayscale. Again, the variation in the profile is small in the central area of the film, varying by only a few percent, and is more significant near the edge of the film (Fig. 9B). Also, the beam profile is not symmetric. The neutron intensity is higher at the top of the film than at the bottom, and drops off more quickly on the left side of the film than the right side.

Plot profiles are taken from both indium and dysprosium radiographs. Fig. 10 shows peak-to-average ratio profiles in the horizontal direction at the beam mid-plane, and Fig. 11 shows profiles in the vertical direction along the center of the beam. There is a notable and unexpected variation in the background profile of the dysprosium foil (thermal neutron)

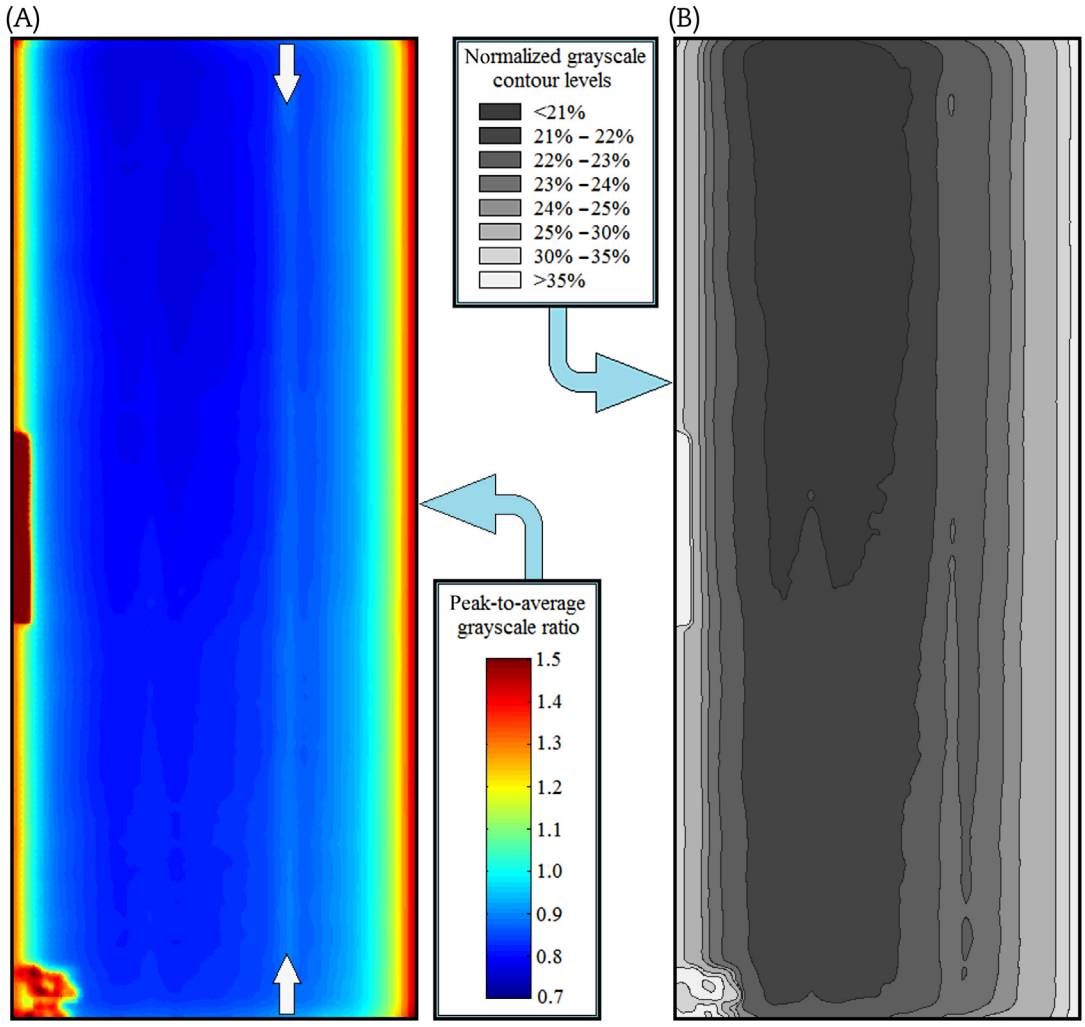

Fig. 9 – Enhanced background image from a dysprosium-exposed film. (A) Peak-to-average ratio two-dimensional mesh plot; (B) normalized 16-bit grayscale contour plot.

image, which can be seen as a decrease in film density running vertically about 12 cm from the left side of the image. This variation is located between the two white arrows in Fig. 9A and indicated in Fig. 10 by the single white arrow. This variation is seen in multiple radiographs taken for this work and in many previous radiographs, including the plot profiles

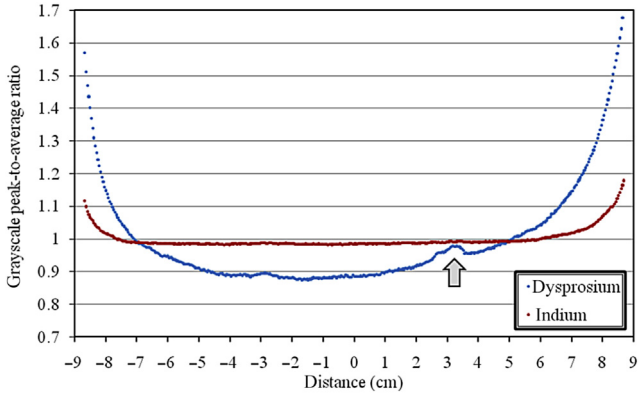

Fig. 10 – Horizontal plot profiles of background radiographs.

produced in previous characterization work [2]. This artifact may have been caused by wet film processing or film digitization using a flatbed scanner, and quality control efforts have been employed to reduce artifacts caused by these processes.

The profile of the dysprosium radiograph in the horizontal direction shows relatively significant variation compared to the profile from the indium foil, which is relatively flat in the horizontal direction (Fig. 10). The beam profile in the vertical direction shows a variation of 5–7% (note the magnitudes of the scales in Figs. 10 and 11). The profile of the dysprosium radiograph in the horizontal direction indicates a 10% decrease in neutron flux from the center to positions 7 cm on either side, similar to the variation observed in the neutron activation gold foils. An additional decrease of 50% is observed at both edges in the horizontal profile, but there are no comparable gold foil results at locations beyond 7 cm from the center. The differences in the beam profiles produced with thermal and epithermal neutrons suggests that the energy spectrum of the neutron beam may not be spatially uniform, in addition to nonuniformity of the flux magnitude. Comparison of the beam profiles is further complicated by the differences in the energy-dependent cross-sections of the materials used in this effort

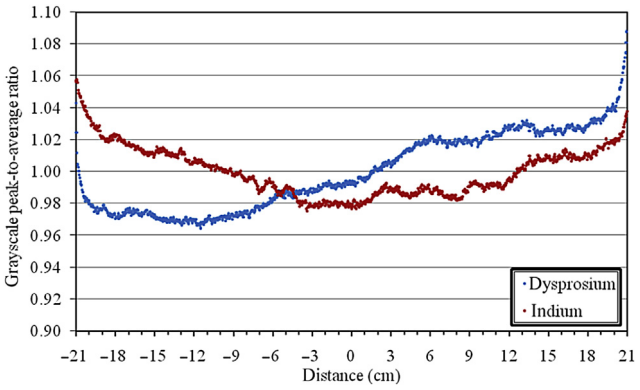

Fig. 11 – Vertical plot profile of background radiographs.

(e.g., gold, dysprosium, indium). Future investigations should evaluate whether the large variation in the horizontal direction away from the center-line is due to variations in the spatial and spectral profiles of the neutron beam or is caused to an artifact of the image transfer process. Future measurements may include activation foils of multiple materials to distinguish the spatial dependence of the neutron energy spectrum. Also, activation foils should be placed over the full area of the image plane to provide beam flux magnitude data at the edges of the beam profile where significant variations are indicated in the background radiographs.

The variation shown in these plot profiles is relatively small in the central portion of the beam and can probably be ignored for most qualitative applications. However, the variations may be significant for some quantitative applications and would require image processing using a light image. Utilizing the characterizations of the ERS neutron beam to remove the background (light image) from the image of a specimen will result in a more accurate interpretation of the specimen in the radiograph.

10. Summary

The NRAD is a 250 kW TRIGA reactor with two neutron beam ports suitable for neutron radiography. The ERS sits beneath the HFEF hot cell, and is used to provide neutron radiography of highly radioactive specimens such as nuclear fuel. Transfer method neutron radiography using dysprosium and indium foils is a gamma-insensitive nondestructive evaluation technique for neutron radiography that provides comprehensive information about the condition of the fuel.

Four new fuel elements were recently added to the NRAD core to increase the excess reactivity. The addition of new fuel could possibly change the neutron beam flux and energy spectrum of the reactor, and the ERS neutron radiography system is characterized per ASTM standards to determine the radiographic category of the facility after the change. Two IQIs are radiographed and analyzed to determine the facility category according to ASTM standards. This work shows that the NRAD ERS neutron radiography system is a Category I facility, the highest quality according to ASTM standards.

To measure the neutron flux and the neutron flux profile, an array of 21 gold foils in a 3 × 7 array are exposed to the neutron beam in the same position as a neutron radiograph would be taken. The experiment is repeated, and the neutron flux is calculated at each location over the area of interest. The neutron flux is generally uniform in the center of the imaging area (~18 cm wide by ~42 cm tall), but has a noticeable variation at the edges in the horizontal direction. The average neutron flux at the image plane with an *L/D* of 125 is 5.96×10^6 n/cm^2/s with a 2σ standard deviation of 2.90×10^5 n/cm^2/s.

Film radiographs taken with dysprosium and indium foil-film transfer method neutron radiography are taken without a specimen in the ERS elevator. These background radiographs are scanned to produce digital 16-bit grayscale images. Profiles are generated using the two background images, which are digitized and image processed to more clearly show the variation in the neutron beam profile. The neutron beam profile varies slightly over the image area and should be taken into account for applications that require quantitative film density measurements from radiographs (or grayscale measurements from the digital scanned image). However, for most qualitative neutron radiography applications, the beam profile can be considered relatively uniform within the central 12.7 cm.

Conflicts of interest

This submitted manuscript was authored by a contractor of the US Government under DOE Contract Number DE-AC07-05ID14517. Accordingly, the publisher, by accepting the article for publication, acknowledges that the US Government retains a nonexclusive, paid-up, irrevocable, worldwide license to publish or reproduce the published form of this manuscript, or allow others to do so, for US Government purposes.

Acknowledgments

The authors acknowledge the R & D staff of the Idaho National Laboratory Materials & Fuels Complex facilities of NRAD, Hot Fuels Examination Facility and Analytical Laboratory for having carried out the experimental tests for this work. This work was performed with support of TerraPower, LLC.

REFERENCES

[1] Idaho National Laboratory, NRAD Safety Analysis Report, Idaho National Laboratory, 2009. DSA-005-NRAD, rev. 5.
[2] S.W. Morgan, J.C. King, C.L. Pope, Beam characterization at the neutron radiography reactor, Nucl. Eng. Des. 265 (2013) 639–653.
[3] S.W. Morgan, J.C. King, C.L. Pope, Simulation of neutron radiograph images at the neutron radiography reactor, Ann. Nucl. Energy 57 (2013) 341–349.
[4] ASTM International, Standard Method for Determining Image Quality in Direct Thermal Neutron Radiographic

Examination, American Society for Testing and Materials, 2005. ASTM E545-05.
[5] J.D. Bess, J.B. Briggs, R.M. Lell, Neutron Radiography (NRAD) Reactor 64-Element Core Upgrade, Idaho National Laboratory, 2014. INL/EXT-13-29628.
[6] J.H. Hubbell, S.M. Seltzer, Tables of X-ray Mass Attenuation Coefficients and Mass Energy-absorption Coefficients from 1 keV to 20 MeV for Elements Z = 1 to 92 and 48 Additional Substances of Dosimetric Interest, National Institute of Standards and Technology, 1995.
[7] M.R. Hawkesworth, J. Walker, Basic principles of thermal neutron radiography, in: J.P. Barton, P. von der Hardt (Eds.), Neutron Radiography, D. Reidel, Dordrecht, Holland, 1983, pp. 5–21.
[8] J.C. Domanus, Control of radiographic image quality in neutron radiography of nuclear fuel, in: 6th International ASM Conference on NDE in Nuclear Industry, Zurich, 1983, pp. 447–451.
[9] V.T. Korneev, K.P. Dubrovin, E.G. Ivanov, The application of neutron radiography for the testing and investigation of nuclear fuel elements, in: J.P. Barton, P. von der Hardt (Eds.), Neutron Radiography, 1983, pp. 375–382. Brussels and Luxembourg.
[10] A. Notea, Y. Segal, F. Trichter, Gap's dimensions in fuel elements from neutron radiography, in: Proceedings of the 6th International ASM Conference on NDE in Nuclear Industry, Zurich, 1983, pp. 433–437.
[11] W.A. Mayer, Investigation of irradiated fuel rods by neutron radiography, Kerntechnik 14 (1972) 343–346.
[12] W.J. Richards, G.C. McClellan, Neutron radiography at the Hot Fuel Examination Facility, in: Proceedings of the 27th Conference on Remote Systems Technology, San Francisco, CA, 1979, pp. 203–208.
[13] W.J. Richards, G.C. McClellan, D.M. Tow, Neutron tomography of nuclear fuel bundles, Mater. Eval. 40 (1982) 1263–1267.
[14] Y. Segal, F. Trichter, Gap width measurements in fuel elements, NDT E Int. 22 (1989) 222–228.
[15] J.C. Domanus, Practical Neutron Radiography, Kluver Academic Publishers, Dordrecht, The Netherlands, 1992.
[16] H. Kobayashi, M. Satoh, Basic performance of a neutron sensitive photo-stimulated luminescence device for neutron radiography, Nucl. Instrum. Methods Phys. Res. A 424 (1999) 1–8.
[17] E.H. Lehmann, G. Frei, G. Kuhne, P. Boillat, The micro-setup for neutron imaging: a major step forward to improve the spatial resolution, Nucl. Instrum. Methods Phys. Res. A 576 (2007) 389–396.
[18] R.L. Cao, S.R. Biegalski, D.S. O'Kelly, A high spatial resolution neutron imaging system using the micro-channel plate detector, in: Neutron Radiography: Proceedings of the Eighth World Conference, DEStech Publications, Inc., Gaithersburg, MD, 2006, pp. 525–535.
[19] A.S. Tremsin, J.B. McPhate, J.V. Vallerga, O.H.W. Siegmund, W.B. Feller, E. Lehmann, L.G. Butler, M. Dawson, High-resolution neutron microtomography with noiseless neutron counting detector, Nucl. Instrum. Methods Phys. Res. A 652 (2011) 400–403.
[20] A.E. Craft, J.C. King, Design, construction, and demonstration of the Colorado School of Mines neutron imaging facility, Nucl. Technol. 184 (2013) 198–209.
[21] B.A. Hilton, S.L. Hayes, Neutron Radiography for Characterizing Irradiated Nuclear Fuels. Nuclear Science Symposium and Medical Imaging Conference (NSS/MIC), IEEE, 2009.
[22] R.H. Bossi, F.A. Iddings, G.C. Wheeler, Nondestructive Testing Handbook vol. 4, Radiographic Testing, American Society for Nondestructive Testing, Inc., USA, 2002.
[23] ASTM International, Standard Practice for Fabrication of the Neutron Radiographic Sensitivity Indicator, American Society for Testing and Materials, 2010. ASTM E2023-10.
[24] ASTM International, Standard Practice for Fabrication of the Neutron Radiographic Beam Purity Indicators, American Society for Testing and Materials, 2010. ASTM E2003-10.
[25] H. Kobayashi, Beam formation and characterization for neutron radiography, Nondest. Test. Eval. 16 (2001) 121–129.
[26] R.R. Greenberg, P. Bode, E.A. De Nadai Fernandez, Neutron activation analysis: a primary method of measurement, Spectrochim Acta Part B At Spectrosc. 66 (2011) 193–241.
[27] ASTM International, Standard Practice for Determining Neutron Fluence, Fluence Rate, and Spectra by Radioactivation Techniques, American Society for Testing and Materials, 2010. ASTM E261-10.
[28] R.F. Fleming, Neutron self-shielding factors for simple geometries, Int. J. Appl. Radiat. Isot. 33 (1982) 1263–1268.
[29] J.K. Shultis, R.E. Faw, Fundamentals of Nuclear Science and Engineering, Marcel Dekker Inc., New York, 2002, p. 105.
[30] R.L. Murri, D.G. Vasilik, A Method to Determine Fast and Thermal Neutron Fluxes by Foil Activation Analysis, The DOW Chemical Company, Rocky Flats Division, RFP-1466, 1971.
[31] R.M. Lindstrom, R.F. Fleming, Neutron self-shielding factors for simple geometries, revisited, Chem. Analityczna 53 (2008) 855–859.